

Equatorial Pacific dust fertilization and source weathering influences on Eocene to Miocene global CO₂ decline

Dunfan Wang^{1,2}, Andrew P. Roberts ³, Eelco J. Rohling ^{3,4}, Weiqi Yao^{1,2}, Yi Zhong^{1,2}, Zhengquan Yao ^{5,6}, Yang Lu¹ & Qingsong Liu^{1,2}✉

Stimulation of the biological pump by iron-bearing dust in the eastern equatorial Pacific Ocean plays an important role in long-term carbon sequestration, yet past dust fertilization and its impact on CO₂ perturbations over major climate transitions remain debated. Here, we integrate proxies of dust input, source-region weathering, and biological pump activity from late Eocene to early Miocene sediments of Integrated Ocean Discovery Program Hole U1333, which includes the Eocene-Oligocene Transition (~34 million years ago) when a major ice sheet was first established on Antarctica. We find that intensified chemical weathering in the large central Asian dust source region enhanced atmospheric CO₂ removal at ~34 Ma. Superimposed dust fertilization and biological pump action amplified this CO₂ removal before ~34 Ma, while weakening of this amplification process helped to moderate the CO₂ decline after that time. The observed inter-linked, counteracting processes with different timescales illustrate the complexity of carbon cycle feedbacks associated with major climate changes.

¹Centre for Marine Magnetism (CM2), Department of Ocean Science and Engineering, Southern University of Science and Technology, Shenzhen 518055, China. ²Southern Marine Science and Engineering Guangdong Laboratory (Guangzhou), Guangzhou, China. ³Research School of Earth Sciences, Australian National University, Canberra ACT 2601, Australia. ⁴School of Ocean and Earth Science, University of Southampton, National Oceanography Centre, Southampton SO14 3ZH, UK. ⁵Key Laboratory of Marine Geology and Metallogeny, First Institute of Oceanography, MNR, Qingdao 266061, China. ⁶Laboratory for Marine Geology, Pilot National Laboratory for Marine Science and Technology, Qingdao 266061, China. ✉email: qslu@sustech.edu.cn

Eolian dust transportation through the atmosphere from land to sea delivers iron to the oceans and facilitates CO₂ removal from the atmosphere by fueling primary productivity and carbon export to the seafloor, which sequesters carbon on geologic timescales¹. Kolber et al.² demonstrated that primary productivity in the eastern equatorial Pacific (EEP) Ocean is limited by the impact of iron on phytoplankton photosynthesis instead of ‘top-down’ grazing pressure by herbivores. This conclusion is supported by iron fertilization experiments in the EEP Ocean, in which the iron released by dust dissolution substantially enhanced ocean primary productivity³. As one of three principal iron-limited high-nutrient, low-chlorophyll (HNLC) ocean regions, it has been proposed that the EEP Ocean plays a crucial role in the global carbon cycle by regulating the rate of CO₂ sequestration from the atmosphere^{4,5}. However, it has also been claimed that ocean dynamics instead of dust input controlled EEP Ocean productivity over the past 0.5 Ma⁶, while inferences of a lack of EEP iron fertilization over the past 10 Ma and the last ice age would seem to negate its role in global carbon sequestration and climate change^{7,8}. Despite great international interest in the relationships between iron fertilization and the carbon cycle^{5–12}, the role of dust fertilization on EEP CO₂ sequestration over major climate transitions remains enigmatic.

Three key questions remain to be clarified. (1) Which iron sources limit EEP productivity and how can they be distinguished from each other? (2) Has the EEP always been iron-limited during the Cenozoic? (3) If so, did iron inputs into the EEP, especially by eolian dust, (partly) regulate atmospheric pCO₂? To address these questions, we collected samples from Integrated Ocean Drilling Program (IODP) Site U1333 Hole B Section 1H-19X (~170-m thick sequence) at ~2 m stratigraphic intervals. Site U1333 is located in the present-day EEP HNLC region (Fig. 1b). By using magnetofossils (the post-mortem remains of magnetotactic bacteria (MTB)) as a palaeoproductivity indicator, we investigate EEP dust fertilization and its role in past atmospheric CO₂ perturbations during the first build-up of major Antarctic glaciation at the EOT. Furthermore, we use chemical weathering information carried by the eolian dust to reconstruct dust source region weathering intensity to assess relationships between continental weathering and global carbon cycling through the greenhouse-to-icehouse transition across the EOT.

Results and discussion

Magnetofossil identification and EEP Ocean dust fertilization.

Reconstructing past EEP Ocean dust fertilization is challenging because of a scarcity of reliable proxies^{9–11}. Opal and total organic carbon (TOC) are used as palaeoproductivity proxies to trace past iron fertilization because they are the remains of microorganisms¹², but they usually fail to constrain relationships between dust inputs and carbon burial in older records due to dissolution and remineralization during settling through the water column and/or sediment burial diagenesis^{6,8,9}. The nano-magnetic remains of MTB, known as magnetofossils¹³, are now recognized to be preserved widely in pelagic sediments and are regarded as a valuable palaeoenvironmental indicator^{14–17}. MTB live near the sediment oxic-anoxic transition zone where iron can be dissolved from detrital particles (e.g., dust) due to sedimentary organic matter degradation, which makes it bioavailable for magnetite biomineralization by MTB¹⁸. Therefore, MTB growth is controlled by the supply of both organic matter and iron to the seafloor. In most cases, the pool of potentially bioavailable iron in sediment is much larger than that consumed for primary productivity. This leads to a bioavailable iron release in sediment that is regulated by the organic carbon flux; thus, MTB growth is limited by export productivity in HNLC oceans¹⁹. Magnetofossil

abundance is, therefore, a useful palaeoproductivity proxy for tracing past dust fertilization in iron-limited oceans.

We measured isothermal remanent magnetizations (IRMs) and first-order reversal curves (FORCs) to detect magnetofossils in the studied sediments²⁰. IRM unmixing results indicate that magnetofossils are dominant along with eolian magnetic minerals with low and high coercivity (Fig. 2). Transmission electron microscope (TEM) observations of extracted magnetic minerals for representative samples corroborate this conclusion. Magnetic mineral inclusions embedded within host silicates are identified in eolian particles alongside polygonal biogenic magnetite particles with variable morphologies. FORC diagrams are used widely to reveal magnetofossil signatures among other magnetic components²¹. FORC results for all analyzed samples have a sharp central ridge along B_u ≈ 0 and a coercivity distribution peak at ~30 mT (Fig. 2g, h), which indicate a dominance of magnetically noninteracting single domain (SD) bacterial magnetite²⁰. Amor et al.²² further developed FORC analysis using micromagnetic calculations and identified distinct magnetofossil signatures for single- and multi-stranded chains using quantile contour lines²³. They found that single-stranded chains have no contribution in the upper half-plane, whereas multi-stranded chains contain additional noncentral ridge contributions in the upper half-plane with slightly asymmetric amplitudes around the central ridge. In our FORC results (Fig. 2a, c, e), the multi-stranded chain signature is more pronounced during the later Eocene and early Miocene when primary productivity was higher than during the Oligocene (Fig. 3a). Magnetofossil morphology and chain configuration are controlled genetically and respond to environmental changes^{17,19}. Our data indicate that limited organic matter supply and iron release may inhibit growth of MTB with multi-stranded chains that produce more magnetic particles, and corroborates the proposed link between carbon export and magnetofossil abundance in marine sediments.

To estimate the relative magnetofossil content in sediments, we measured the anhysteretic remanent magnetization after alternating field demagnetization at 20 mT (ARM_{@20 mT}), which is sensitive to the stable SD ferrimagnetic particle concentration²⁴. No eolian magnetite with SD size was observed in TEM images. However, SD magnetic minerals could also occur as inclusions within silicate hosts, which would contribute to the ARM_{@20 mT} signal²⁵. This contribution can be separated by chemical treatment (10 mol/L hydrochloric acid with 24 h reaction time) in which biogenic and unprotected phases will be removed efficiently but silicate-hosted magnetic inclusions will be largely preserved²⁶. Therefore, we compare ARM_{@20 mT} for the same samples before and after chemical treatment to quantify magnetofossil and silicate inclusion contributions to ARM_{@20 mT}. For all representative samples, magnetofossil contributions to ARM_{@20 mT} exceed 95% (Supplementary Fig. 1). Thus, ARM_{@20 mT} provides a reliable representation of sedimentary magnetofossil contents here.

A dust record was obtained by determining the hard (>300 mT) isothermal remanent magnetization (HIRM_{300 mT}) and the ‘operationally defined eolian dust’ (ODED). After removing authigenic marine components by conducting a sequential chemical extraction, the residual material mainly contains refractory silicates that are regarded as ODED²⁷. Ideally, ODED is the product of upper continental crustal weathering, but volcanic ash can also survive in the chemical residue²⁸. This can be identified and quantified geochemically using La-Th-Sc diagrams^{29,30}. La-Th-Sc results indicate that volcanic ash apparently has little effect on our record (Supplementary Fig. 2). We also measured total Fe, opal, and TOC for bulk sediments to quantify the relationship between iron supply and export productivity. Coincident eolian dust and bulk sediment Fe variations with strong correlation between Fe and ODED suggest that sedimentary iron was supplied mainly by

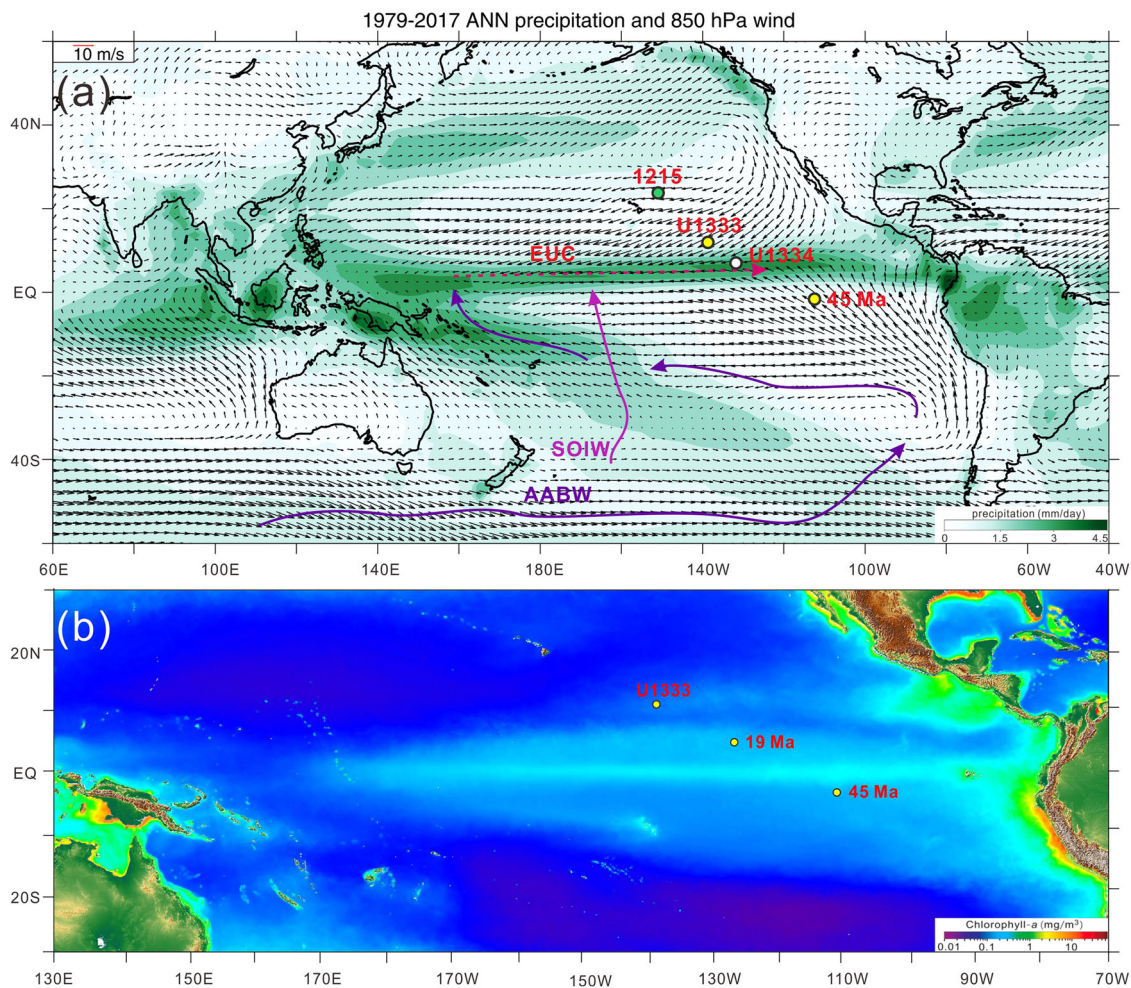


Fig. 1 Location map. **a** Overview of wind fields⁶³ and the Pacific Ocean current system⁶⁴. Yellow circles indicate the modern (10.52°N, 138.42°W) and past position of Site U1333 at 45 Ma (3.95°S, 111.20°W). White and green circles indicate the locations of Site U1334 and Site 1215, respectively. Antarctic Bottom Water (AABW) and Southern Ocean Intermediate Water (SOIW) transports nutrients to the EEP by the Equatorial undercurrent (EUC). **b** Surface chlorophyll concentration reflects primary production (oceancolor.gsfc.nasa.gov/SEAWIFS). Site U1333 is located within the modern high-nutrient, low-chlorophyll (HNLC) zone; palaeo-locations at 45 and 19 Ma are after Parés and Moore⁶⁵.

terrestrial eolian dust (Fig. 3b)²⁷. It has been argued that EEP primary productivity might be enhanced by iron supplied by upwelling³¹, which fundamentally depends on ocean circulation and wind patterns. However, strong correlation between Fe and terrigenous material (ODED) in our record suggests a dominant impact of dust on iron supply, as does consistent variations between dust input and magnetofossil abundance. Thus, we propose that eolian dust is the major external iron source to the EEP, and that the iron released from this material stimulated EEP primary productivity from the later Eocene to early Miocene. Opal and TOC do not correlate well with Fe, which suggests their limited potential as productivity proxies here, likely due to poor preservation⁹. In contrast, we find magnetofossil content to be a more reliable productivity proxy for tracing ancient dust fertilization.

ITCZ migration and dust source region humidification. Marine sedimentary dust records contain important information about source environments and provide a window on past climate changes³². Dust from the second largest global dust source region, the Asian interior, can be transported eastward by wind to the Chinese Loess Plateau, North Pacific Ocean, and even the EEP Ocean³³. Seo et al.³⁴ identified dust from the Asian interior and

south/central America by studying surface sediment geochemical properties in the central Pacific Ocean. Using the concentration of light rare earth elements (LREE) relative to heavy rare earth elements (represented by the La_N/Yb_N ratio), they found that dust provinces north and south of the Intertropical Convergence Zone (ITCZ) are LREE enriched and depleted, respectively. In our study, all ODED La_N/Yb_N data fall within the enriched LREE range, as expected for Asian dust (Fig. 4a). First, this indicates that EEP dust was derived mainly from the Asian interior and, second, that the ITCZ was located south of the equator by at least 4° during the Eocene (~45 Ma) because Asian dust would not have been able to reach the studied core site (palaeolatitude ~3.95°S at 45 Ma) if the ITCZ was located to the north of the site (Fig. 1a).

The ITCZ, which marks the convergence of southeasterly and northeasterly trade winds, forms a powerful convective boundary for dust transportation and deposition to the EEP Ocean³⁵. It has been suggested that the ITCZ shifts in response to global cooling, which would affect EEP dust transportation and deposition patterns^{34–36}. An EEP dust record from Site U1334 (palaeolatitude ~0.38°S at 34 Ma) reveals that its dust source changed across the EOT from the Asian interior to South America, which

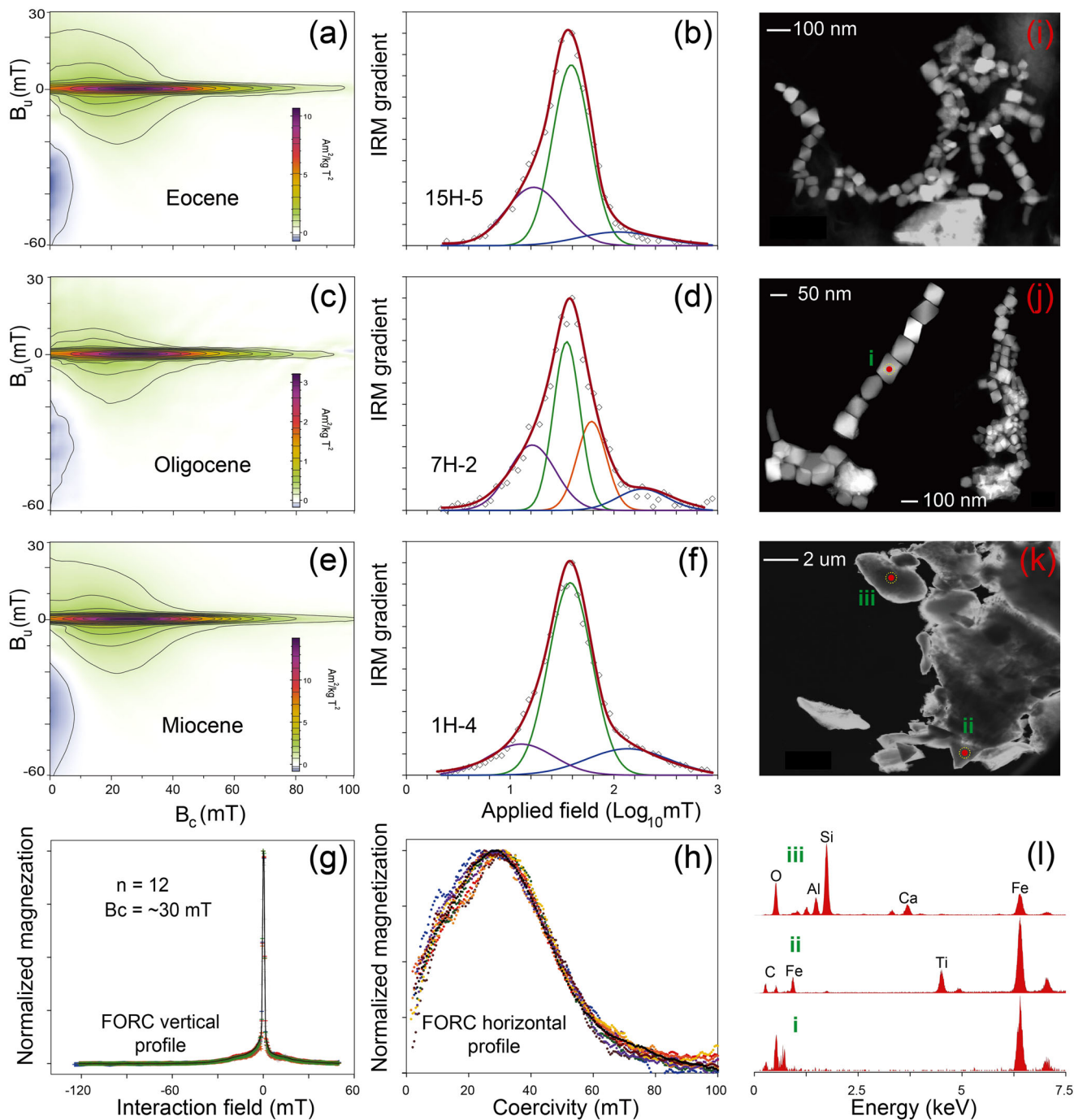


Fig. 2 Magnetofossil identification using magnetic and TEM analysis. **a–f** FORC diagrams and IRM component analysis for representative Eocene, Oligocene, and Miocene samples. The derivative of IRM acquisition curves is plotted as open diamond symbols. Fitted components have different colors: red, sum of fitted components; green and orange, biogenic soft and hard magnetite, respectively, with narrow distributions; purple and blue, low- and high-coercivity detrital magnetic assemblages with broader distributions, respectively (for more details see Supplementary Table 1). **g, h** Vertical and horizontal profiles of FORC diagrams, respectively, for selected samples. **i–l** TEM images and EDXS analyses (numbered dots) of magnetofossils with different morphologies and irregularly shaped eolian dust particles.

indicates that the ITCZ shifted northward during that time of global cooling and Antarctic ice-sheet expansion³⁷. Our results indicate that Site U1333 (palaeolatitude $\sim 2.91^\circ$ S at 34 Ma) remained a sink for Asian dust after the EOT. Hence, combined results from U1333 and U1334 constrain the EOT ITCZ palaeolatitude shift to at most $\sim 2.5^\circ$ (Supplementary Fig. 3).

Global hydroclimate changed markedly across the EOT³⁸. With ice-sheet expansion, Asian interior conditions changed dramatically. For example, it has been reported that aridification was

enhanced and monsoon rainfall declined across the EOT in the Asian interior because prevailing westerlies transported less moisture to Central Asia with Neotethys Ocean retreat^{39,40}. Conversely, ancient soils and carbonate nodules (formed by chemical eluviation) in eolian red clay strata suggest that the Asia interior was moister after the EOT⁴¹. The chemical index of alteration (CIA) is a useful weathering index to reconstruct source climate conditions⁴². Higher CIA values usually indicate enhanced chemical weathering in moister source areas, whereas lower values

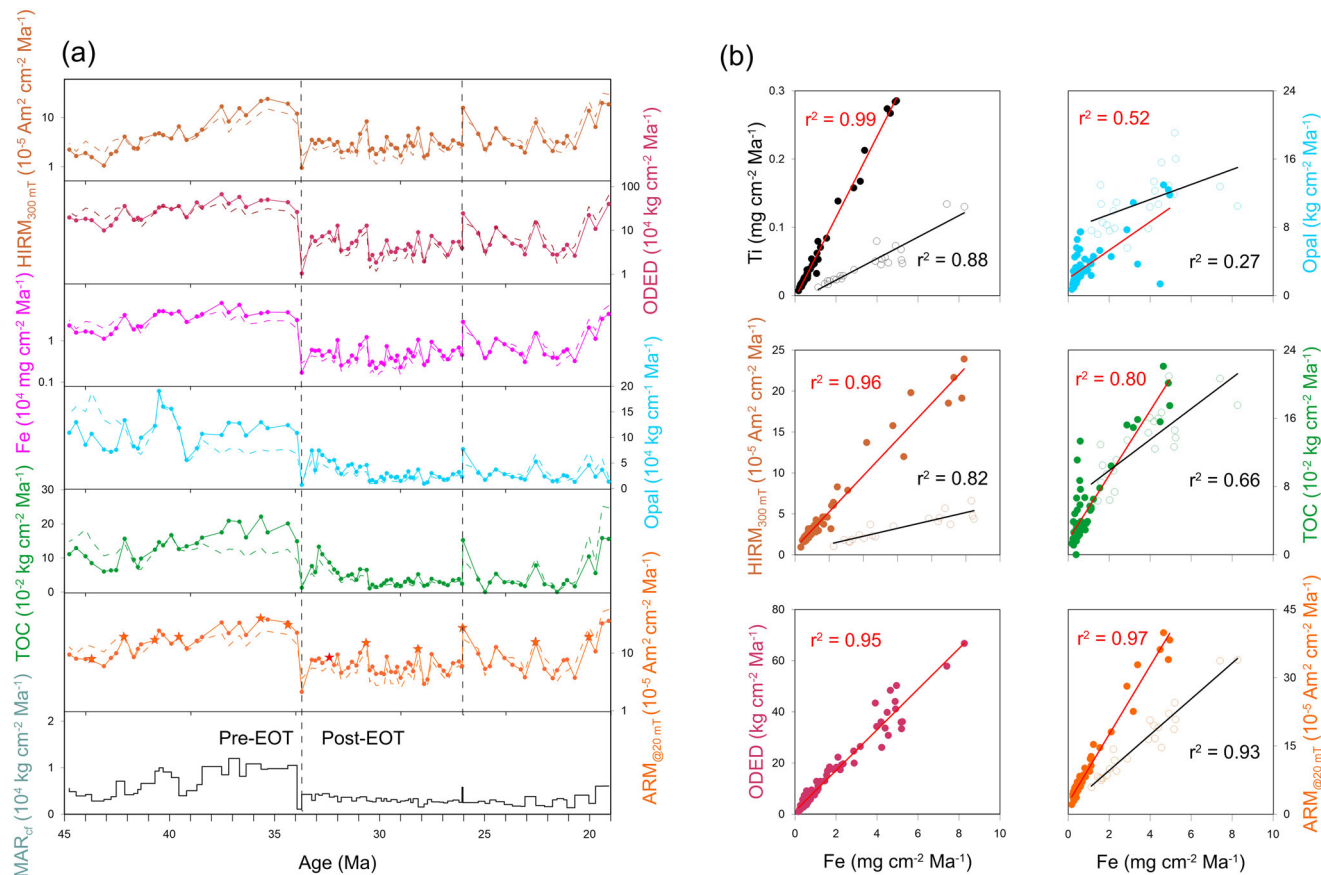


Fig. 3 Dust, productivity, and total Fe record for Site U1333. **a** Variations of dust, iron, and productivity. Vertical dashed lines mark the boundaries between the Eocene, Oligocene, and Miocene. Each parameter is shown in flux and dash line represents the content, HIRM_{300 mT} and ARM_{@20 mT} were calculated on a carbonate-free basis. Star symbols in the ARM_{@20 mT} panel represent samples selected for FORC and IRM measurements. **b** Correlations between Fe and terrigenous (ODED, HIRM_{300 mT}, and Ti), and biogenic (ARM_{@20 mT}, TOC, and opal) components shown in **a**; black and red lines represent pre- and post-EOT correlations, respectively.

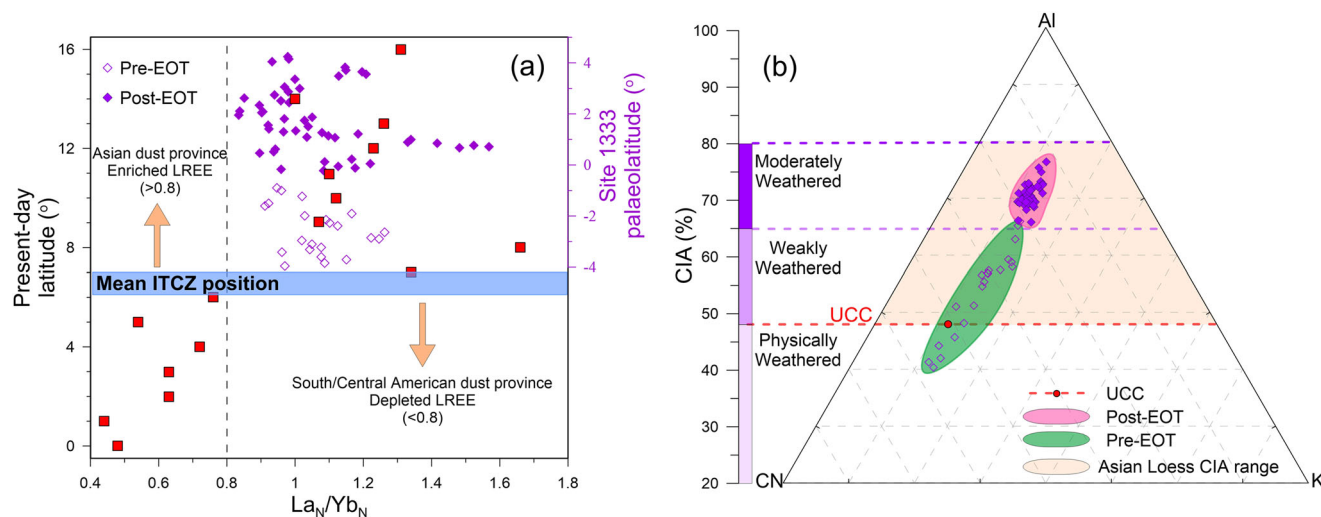


Fig. 4 Dust source regions and CIA pattern. **a** Mean ITCZ position and EEP dust regimes defined using the La_N/Yb_N ratio. Red squares: data for 16 sediment cores with respect to latitude from the equator to 16°N along 131.5°W longitude in the central Pacific Ocean³⁴; open and solid rhombi: pre- and post-EOT data from ODED at Site U1333. **b** Al-CN-K ($Al_2O_3 - CaO + Na_2O - K_2O$) diagram for Site U1333 and CIA ranges of UCC and Asian Loess refer to Zhang et al.⁴⁵ and Taylor and McLennan⁶⁰.

suggest a predominance of physical weathering processes⁴³. Although chemical weathering can be influenced by provenance, diagenesis, and sorting during transportation, careful sampling and reasonable exclusion can yield important information about

the source environment^{44,45}. Here, to ensure CIA reliability for inferring environmental changes in dust source areas, we assess potential dust provenance changes by measuring the $^{143}Nd/^{144}Nd$ ratio (ϵ_{Nd}). All ODED ϵ_{Nd} values (Supplementary Table 2) vary

within the range expected for the central Asian orogen (CAO) (Supplementary Fig. 4), which suggests a single Asian dust source region for Site U1333. Moreover, palaeogeographic and tectonic reconstructions across the EOT suggest that the Paratethys Sea still existed and that the Tarim and Qaidam Basins supported continental-lacustrine sedimentation at that time, which suggest that the northern Tibetan plateau (NTP) dust source had not formed^{46–48}. Thus, dust from Site U1333 was mainly derived from a single Asian interior source region, such as the Mongolian Gobi (MG) deserts. Our ODED CIA data have the expected characteristics of eolian deposition from the Asian interior, similar to coeval Inner Mongolian dust deposits (Supplementary Fig. 5)⁴⁹. These characteristics include (a) a nearly parallel distribution along the CN–Al (CaO*+Na₂O–Al₂O₃) trend, which suggests weak K-metasomatism (K₂O) and negligible diagenetic influences^{43,44}, and (b) the same value range as Mongolian deposits across the EOT, which suggests an absence of obvious sorting influence. Overall, therefore, our CIA results appear to provide a reliable record of major central Asian environmental changes.

Our CIA results indicate contrasting conditions across the EOT (Fig. 4b); all pre-EOT data lie below the moderate weathering threshold, while all post-EOT data fall above it. This suggests that the dust source region became moister with enhanced chemical weathering after the EOT. It has been suggested that dust source regions could have been wetter during glacial periods with meltwater from alpine snow and glacier melt facilitating chemical weathering⁴⁵. Although the EOT was marked by Antarctic glacial build-up, evidence of intermittent northern hemisphere cooling with high-altitude snow and glacial ice has also been reported^{50–52}. Intermittent seasonal meltwater and reduced evaporation under colder conditions would have made dust source regions moister after the EOT and promoted chemical weathering at this time of global cooling.

Increased chemical weathering (from weak to moderate) across the EOT is also consistent with the increased linear slope between Fe and Ti, and Fe and HIRM_{300 mT} before and after the EOT (Fig. 3b). Fe²⁺ is more easily leached from silicates than Ti³⁺, so intensified source region chemical weathering after the EOT would have caused more iron to leach out from extracted dust materials (ODED) to drive a Ti/Fe increase. Similarly, iron oxidation would form more hematite and contribute to HIRM_{300 mT}, which would cause HIRM_{300 mT}/Fe to increase²⁴. Magnetofossil abundance (ARM_{@20 mT}) has the same slope difference before and after the EOT. This suggests that the EOT represents a compositional turning point for eolian dust, with post-EOT dust containing more bioavailable iron than pre-EOT dust. This bioavailable iron increase corresponds to the order of magnitude chemical weathering increase after the EOT and indicates that the HIRM_{300 mT} dust proxy is more representative of potential bioavailable iron from dust. Opal and TOC also have an increased slope after the EOT, but they are less consistent with the magnetofossil record, which suggests that they have limited value for tracing past dust fertilization due to the preservation issues mentioned above⁹. Iron fertilization stimulates primary productivity, but diatoms and other planktonic carbon sources have the risk of becoming food for larger organisms or fuel for microbes as they sink through the water column.

Impact of continental weathering and dust fertilization on global CO₂ decline. Palaeogeographic reconstructions indicate that central Asian orogenic uplift had begun at ~50 Ma and that most of the Tibetan Plateau was elevated by the Eocene, ~40 million years ago, well before the EOT⁵⁴. Tectonic activity can produce steeper slopes and fresh surface rock exposures, which would promote continental weathering⁵⁵. Our linked atmospheric

CO₂ and CIA trends from the late Eocene to early Miocene support the suggestion that continental weathering exerts an important control on the global carbon cycle on tectonic timescales (Fig. 5e, f), and that central Asian orogenic uplift may have played an important role in global climate change⁵⁶. Moreover, we find that the EOT was a change point between relatively weak and moderate weathering (Fig. 4b). This, combined with an order of magnitude humidification increase and the size of central Asia, suggests that intensified carbon sequestration due to increased regional weathering rates may have been an important contributor to global CO₂ decline, and thus to icehouse climate development across the EOT.

Our results indicate that a strong biological pump (including sedimentary C_{org} burial) fueled by dust inputs aided atmospheric CO₂ drawdown from the late Eocene to early Miocene (Fig. 5c, f). However, a prominent dust decline across the EOT that coincided with the onset of Antarctic glaciation at ~34 Ma (Fig. 5d) weakened the dust-fueled biological pump and CO₂ fixation efficiency in the EEP after the EOT. We propose that weakening of EEP dust fertilization across the EOT moderated the global EOT CO₂ decline. This would have acted alongside a suggested moderating mechanism for the EOT CO₂ decline in which sea-level drop caused oxidation of exposed sulfide minerals on continental shelves and subsequent carbonate dissolution that released CO₂⁵⁷. Together, these processes dampened, but did not negate, the CO₂ decline across the EOT.

Conclusions

We demonstrate that magnetofossils are a valuable proxy for dust fertilization in the eastern equatorial Pacific (EEP) Ocean and for carbon burial over geological timescales. We demonstrate this with co-registered records (i.e., identical samples) of EEP biological pump activity, dust inputs, and chemical weathering proxies from the late Eocene to early Miocene. Our results reveal intricate connections between Asian interior conditions and EEP dust fertilization across a marked global climate transition, the Eocene–Oligocene Transition (EOT), over which major Antarctic glaciation initiated. We also find that intensified chemical weathering in large central Asian dust source regions augmented atmospheric CO₂ removal, whereas decreasing EEP dust fertilization and biological pump action presented a moderating feedback on the EOT CO₂ decline.

Methods

Magnetic measurements and transmission electron microscope observations.

IRM curves were measured at 80 logarithmically spaced field steps, and were unmixed using a one-dimensional Gaussian mixing model in the “pyIRM” software (available at <https://github.com/botaoxiengyong/pyIRM>). Up to 201 FORCs were measured with 300–400 ms averaging times; data were processed using VARIFORC with $s = 2$ across the central ridge, and $s = 5$ and $\lambda 0.08$ over the remaining parts⁵⁸. The data were measured using a vibrating sample magnetometer (VSM, Princeton MicroMag 3900). Samples were prepared for transmission electron microscope (TEM) observations with energy-dispersive X-ray spectroscopy (EDXS) analyses of magnetic mineral extracts to identify magnetic minerals. An anhysteretic remanent magnetization (ARM) was imparted by superimposing a 0.05 mT direct current (DC) bias field on a smoothly decreasing 100 mT peak alternating field (AF), which was then demagnetized with a 20 mT peak AF to obtain ARM_{@20 mT}. For the same samples, an eolian dust record was obtained by determining the ‘hard (>300 mT)’ isothermal remanent magnetization: HIRM_{300 mT} = (SIRM_{1.2 T} – IRM_{300 mT}) × 0.5, where –IRM_{300 mT} is the isothermal remanent magnetization (IRM) produced in a 300 mT backfield after applying a saturation IRM in a 1.2 T forward field (SIRM_{1.2 T}). HIRM_{300 mT} reflects the high-coercivity hematite and goethite contribution that is widely regarded as an eolian dust indicator²⁷.

Geochemical sequential extractions and analyses. ‘Operationally defined eolian dust’ (ODED) was obtained by conducting a sequential chemical extraction from the bulk sediment (Supplementary Table S3). Geochemical properties of these refractory silicates were measured to discriminate potential ODED sources and to assess the chemical index of alteration (CIA), which is calculated in molecular proportions: CIA = [Al₂O₃/(Al₂O₃ + CaO* + Na₂O + K₂O)]*100, where CaO* is

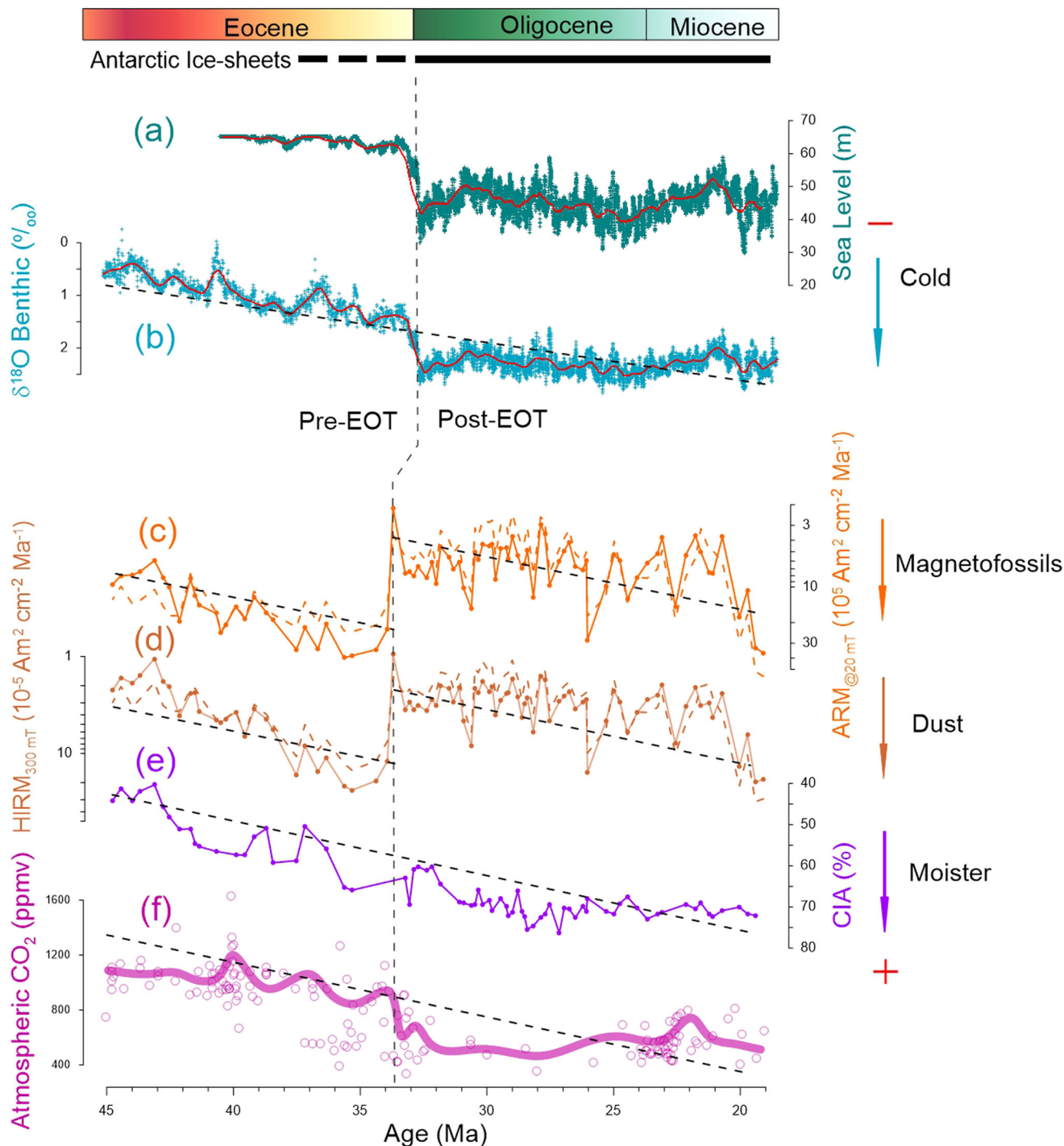


Fig. 5 Global climate changes, EEP dust fertilization, and source weathering. **a, b** Sea level and benthic foraminiferal $\delta^{18}\text{O}$ variations^{50,66}. **c–e** Productivity (magnetofossils), eolian dust, and CIA records, respectively, for Site U1333. **f** Synchronous atmospheric CO_2 variations⁶⁷ (solid line = five-point running average). $\delta^{18}\text{O}$, productivity, eolian dust, CIA, and CO_2 have the same trend; a sharp dust input reduction coincides with biological pump weakening across the EOT.

the amount of CaO incorporated in siliceous rock⁴². Measured CaO contents due to Ca in phosphates (apatite) were corrected following McLennan⁵⁹. Hemispheric EEP dust source regions are differentiated by normalized La/Yb ratios, expressed as $\text{La}_N/\text{Yb}_N = (\text{La}/\text{Yb})_{\text{sample}}/(\text{La}/\text{Yb})_{\text{PAAS}}$, where PAAS is post-Archean Australian average shale⁶⁰. A single Asian interior dust source is identified using Nd isotopic ratios; data are reported as ϵ_{Nd} relative to the chondrite uniform reservoir⁶¹ where $\epsilon_{\text{Nd}} = [({}^{143}\text{Nd}/{}^{144}\text{Nd} - 0.512638) \div 0.512638] \times 10^4$.

To assess the reliability of our magnetofossil indicator ($\text{ARM}_{@20\text{mT}}$), we conducted a chemical demagnetization experiment on representative samples to quantify single domain (SD) magnetic inclusion contributions to the $\text{ARM}_{@20\text{mT}}$ signal within silicates carried by dust^{25,26}. Sediment ages were obtained by linear interpolation using the timescale of Westerhold et al.⁶² (Supplementary Fig. 6).

Eolian dust, iron, TOC, opal, and $\text{ARM}_{@20\text{mT}}$ fluxes were calculated by multiplication with the mass accumulation rate (MAR), where $\text{MAR} = \text{density} * \text{LSR}$ (linear sedimentation rate). The carbonate-free MAR reflects carbonate compensation depth changes expressed as $\text{MAR}_{\text{cf}} = \text{MAR} * (1 - \text{CaCO}_3\% \text{ wt})$. (for details, see Supplementary Note 1).

Data availability

The data set supporting this study includes chemical composition, rock magnetic, isothermal remanent magnetization (IRM) unmixing and Nd isotopic results are available in the publically accessible repository at <https://doi.org/10.5281/zenodo.7601454>.

Received: 5 June 2022; Accepted: 3 February 2023;

Published online: 15 February 2023

References

- Jickells, T. D. et al. Global iron connections between desert dust, ocean biogeochemistry, and climate. *Science* **308**, 67–71 (2005).
- Kolber, Z. S. et al. Iron limitation of phytoplankton photosynthesis in the equatorial Pacific Ocean. *Nature* **371**, 145–148 (1994).
- Coale, K. H. et al. A massive phytoplankton bloom induced by an ecosystem-scale iron fertilization experiment in the equatorial Pacific Ocean. *Nature* **383**, 495–501 (1996).
- Martin, J. H. Glacial-interglacial CO₂ change: the iron hypothesis. *Paleoceanography* **5**, 1–13 (1990).
- Erhardt, A. M. Palaeoceanography: tropical ties. *Nat. Geosci.* **10**, 714–715 (2017).
- Winckler, G., Anderson, R. F., Jaccard, S. L. & Marcantonio, F. Ocean dynamics, not dust, have controlled equatorial Pacific productivity over the past 500,000 years. *Proc. Natl. Acad. Sci. USA* **113**, 19–24 (2016).
- Ziegler, C. L., Murray, R. W., Plank, T. S. & Hemming, R. Sources of Fe to the equatorial Pacific Ocean from the Holocene to Miocene. *Earth Planet. Sci. Lett.* **270**, 258–270 (2008).
- Costa, K. M. et al. No iron fertilization in the equatorial Pacific Ocean during the last ice age. *Nature* **529**, 519–522 (2016).
- Lyle, M. Bloom without fertilizer. *Nat. Geosci.* **1**, 576–578 (2008).
- Jacobel, A. W., Anderson, R. F., Winckler, G., Costa, K. M. & Zhou, Y. No evidence for equatorial Pacific dust fertilization. *Nat. Geosci.* **12**, 154–155 (2019).
- Marcantonio, F., Loveley, M. R., Schmidt, M. W. & Hertzberg, J. E. Reply to: No evidence for equatorial Pacific dust fertilization. *Nat. Geosci.* **12**, 156–156 (2019).
- Murray, R. W., Leinen, M. & Knowlton, C. W. Links between iron input and opal deposition in the Pleistocene equatorial Pacific Ocean. *Nat. Geosci.* **5**, 270–274 (2012).
- Kirschvink, J. L. & Chang, S. R. Ultrafine-grained magnetite in deep-sea sediments: possible bacterial magnetofossils. *Geology* **12**, 559–562 (1984).
- Roberts, A. P. et al. Magnetic properties of pelagic marine carbonates. *Earth-Sci. Rev.* **127**, 111–139 (2013).
- Chang, L. et al. Coupled microbial bloom and oxygenation decline recorded by magnetofossils during the Palaeocene–Eocene Thermal Maximum. *Nat. Commun.* **9**, 4007 (2018).
- Lu, Y. et al. Paleoenvironmental significance of magnetofossils in pelagic sediments in the equatorial Pacific Ocean before and after the Eocene/Oligocene boundary. *J. Geophys. Res.: Solid Earth* **126**, e2021JB022221 (2021).
- Li, J. H. et al. Bullet-shaped magnetite biomineralization within a magnetotactic *Deltaproteobacterium*: implications for magnetofossil identification. *J. Geophys. Res.: Biogeosciences* **125**, e2020JG005680 (2020).
- Roberts, A. P. Magnetic mineral diagenesis. *Earth-Sci. Rev.* **151**, 1–47 (2015).
- Roberts, A. P. et al. Magnetotactic bacterial abundance in pelagic marine environments is limited by organic carbon flux and availability of dissolved iron. *Earth Planet. Sci. Lett.* **310**, 441–452 (2011).
- Egli, R., Chen, A. P., Winklhofer, M., Kodama, K. P. & Horng, C. S. Detection of noninteracting single domain particles using first-order reversal curve diagrams. *Geochem. Geophys. Geosyst.* **11**, Q01Z11 (2010).
- Roberts, A. P., Pike, C. R. & Verosub, K. L. First-order reversal curve diagrams: a new tool for characterizing the magnetic properties of natural samples. *J. Geophys. Res.: Solid Earth* **105**, 28461–28475 (2000).
- Amor, M. et al. Key signatures of magnetofossils elucidated by mutant magnetotactic bacteria and micromagnetic calculations. *J. Geophys. Res.: Solid Earth* **127**, e2021JB023239 (2022).
- Egli, R. Magnetic characterization of geologic materials with first-order reversal curves in Magnetic Measurement Techniques for Materials Characterization (eds. Franco, V. & Dodrill, B.) 455–600 (Springer Nature, 2021).
- Liu, Q. S. et al. Environmental magnetism: principles and applications. *Rev. Geophys.* **50**, RG4002 (2012).
- Chang, L. et al. Widespread occurrence of silicate-hosted magnetic mineral inclusions in marine sediments and their contribution to paleomagnetic recording. *J. Geophys. Res.: Solid Earth* **121**, 8415–8431 (2016).
- Jiang, X. D. et al. Quantifying contributions of magnetic inclusions within silicates to marine sediments: a dissolution approach to isolating volcanic signals for improved paleoenvironmental reconstruction. *J. Geophys. Res.: Solid Earth* **126**, e2021JB022680 (2021).
- Zhang, Q., Liu, Q. S., Li, J. & Sun, Y. B. An integrated study of the eolian dust in pelagic sediments from the North Pacific Ocean based on environmental magnetism, transmission electron microscopy, and diffuse reflectance spectroscopy. *J. Geophys. Res.: Solid Earth* **123**, 3358–3376 (2018).
- Ziegler, C. L., Murray, R. W., Hovan, S. A. & Rea, D. K. Resolving eolian, volcanogenic, and authigenic components in pelagic sediment from the Pacific Ocean. *Earth Planet. Sci. Lett.* **254**, 416–432 (2007).
- Olivarez, A. M., Owen, R. M. & Rea, D. K. Geochemistry of eolian dust in Pacific pelagic sediments: implications for paleoclimatic interpretations. *Geochim. Cosmochim. Acta* **55**, 2147–2158 (1991).
- Weber, E. T. et al. Quantitative resolution of eolian continental crustal material and volcanic detritus in North Pacific surface sediment. *Paleoceanography* **11**, 115–127 (1996).
- Coale, K. H., Steven, E., Fitzwater, R. & Michael, G. Control of community growth and export production by upwelled iron in the equatorial Pacific Ocean. *Nature* **379**, 621–624 (1996).
- Wan, S. M., Sun, Y. B. & Nagashima, K. Asian dust from land to sea: processes, history and effect from modern observation to geological records. *Geol. Mag.* **157**, 701–706 (2020).
- An, Z. S. Late Cenozoic Climate Change in Asia: Loess, Monsoon and Monsoon-Arid Environment Evolution (ed. An, Z. S.) 1–587 (Springer, New York, 2014).
- Seo, I., Kim, M. G., Yoo, C. M. & Hyeong, K. Geochemically defined mean position of the Intertropical Convergence Zone in the central Pacific. *Geophys. Res. Lett.* **48**, e2021GL094432 (2021).
- Reimi, M. A. & Marcantonio, F. Constraints on the magnitude of the deglacial migration of the ITCZ in the Central Equatorial Pacific Ocean. *Earth Planet. Sci. Lett.* **453**, 1–8 (2016).
- Yamazaki, T. Paleoposition of the Intertropical Convergence Zone in the eastern Pacific inferred from glacial-interglacial changes in terrigenous and biogenic magnetic mineral fractions. *Geology* **40**, 151–154 (2012).
- Hyeong, K., Kuroda, J., Seo, I. & Wilson, P. A. Response of the Pacific inter-tropical convergence zone to global cooling and initiation of Antarctic glaciation across the Eocene Oligocene Transition. *Sci. Rep.* **6**, 30647 (2016).
- Ao, H. et al. Orbital climate variability on the northeastern Tibetan Plateau across the Eocene-Oligocene transition. *Nat. Commun.* **11**, 5249 (2020).
- Sun, J. M. & Windley, B. F. Onset of aridification by 34 Ma across the Eocene–Oligocene transition in Central Asia. *Geology* **43**, 1015–1018 (2015).
- Page, M. et al. Synchronous cooling and decline in monsoonal rainfall in northeastern Tibet during the fall into the Oligocene icehouse. *Geology* **47**, 203–206 (2019).
- Sun, J. M., Liu, W. G., Liu, Z. H. & Fu, B. H. Effects of the uplift of the Tibetan Plateau and retreat of Neotethys Ocean on the stepwise aridification of mid-latitude Asian interior. *Bull. Chin. Acad. Sci.* **32**, 951–958 (2017).
- Nesbitt, H. W. & Young, G. M. Prediction of some weathering trends of plutonic and volcanic rocks based on thermodynamic and kinetic considerations. *Geochim. Cosmochim. Acta* **48**, 1523–1534 (1984).
- Fedo, C. M., Nesbitt, H. W. & Young, G. M. Unraveling the effects of potassium metasomatism in sedimentary rocks and paleosols, with implications for paleoweathering conditions and provenance. *Geology* **23**, 921–924 (1995).
- Bahlburg, H. & Dobrzinski, N. A review of the chemical index of alteration (CIA) and its application to the study of Neoproterozoic glacial deposits and climate transitions. In *The Geological Record of Neoproterozoic Glaciations* (eds. Arnaud, E., Halverson, G. P. & Shields, G. A.) 81–92 (Geological Society, 2011).
- Zhang, Q. et al. Mechanism for enhanced eolian dust flux recorded in North Pacific Ocean sediments since 4.0 Ma: aridity or humidity at dust source areas in the Asian interior? *Geology* **48**, 77–81 (2020).
- Zheng, H. B. et al. Late Oligocene–early Miocene birth of the Taklimakan Desert. *Proc. Natl. Acad. Sci. USA* **112**, 7662–7667 (2015).
- Wu, M. H., Zhuang, G. S., Hou, M. & Liu, Z. Expanded lacustrine sedimentation in the Qaidam Basin on the northern Tibetan Plateau: manifestation of climatic wetting during the Oligocene icehouse. *Earth Planet. Sci. Lett.* **565**, 116935 (2021).
- Zhang, J. Y. et al. Palaeogeographic reconstructions of the Eocene-Oligocene Tarim Basin (NW China): sedimentary response to late Eocene sea retreat. *Palaeogeogr. Palaeoclimatol. Palaeoecol.* **587**, 110796 (2022).
- Wasiljeff, J. et al. Oligocene moisture variations as evidenced by an aeolian dust sequence in Inner Mongolia, China. *Sci. Rep.* **12**, 5597 (2022).
- Rohling, E. J. et al. Sea level and deep-sea temperature reconstructions suggest quasistable states and critical transitions over the past 40 million years. *Sci. Adv.* **7**, eabf5326 (2021).
- Zanazzi, A., Kohn, M. J., MacFadden, B. J. & Terry, D. O. Large temperature drop across the Eocene–Oligocene transition in central North America. *Nature* **445**, 639–642 (2007).
- Hutchinson, D. K. et al. The Eocene–Oligocene transition: a review of marine and terrestrial proxy data, models and model–data comparisons. *Clim. Past* **17**, 269–315 (2021).
- Nesbitt, H. W. & Markovics, G. Weathering of granodioritic crust, long-term storage of elements in weathering profiles, and petrogenesis of siliciclastic sediments. *Geochim. Cosmochim. Acta* **61**, 1653–1670 (1997).

54. Botsyun, S. et al. Revised paleoaltimetry data show low Tibetan Plateau elevation during the Eocene. *Science* **363**, 946–946 (2019).
55. Goudie, A. S. & Viles, H. A. Weathering and the global carbon cycle: geomorphological perspectives. *Earth-Sci. Rev.* **113**, 59–71 (2012).
56. Gernon, T. M. et al. Global chemical weathering dominated by continental arcs since the mid-Palaeozoic. *Nat. Geosci.* **14**, 690–696 (2021).
57. Yao, W. Q., Markovic, S., Paytan, A., Erhardt, A. M. & Wortmann, U. G. Quantifying pyrite oxidation on continental shelves during the onset of Antarctic glaciation in the Eocene–Oligocene transition. *Earth Planet. Sci. Lett.* **568**, 117015 (2021).
58. Egli, R. VARIFORC: an optimized protocol for calculating non-regular first-order reversal curve (FORC) diagrams. *Glob. Planet. Change* **110**, 302–320 (2013).
59. McLennan, S. M. Weathering and global denudation. *J. Geol.* **101**, 295–303 (1993).
60. Taylor, S. R. & McLennan, S. M. *The Continental Crust: Its Composition and Evolution.* (Blackwell, Massachusetts, 1985).
61. Jacobsen, S. B. & Wasserburg, G. J. Sm–Nd isotopic evolution of chondrites. *Earth Planet. Sci. Lett.* **50**, 139–155 (1980).
62. Westerhold, T. & The Expedition 320/321 Scientists. Revised composite depth scales and integration of IODP Sites U1331–U1334 and ODP Sites 1218–1220. Proceedings of the Integrated Ocean Drilling Program 320/321 (2012).
63. Kanamitsu, M. et al. NCEP–DOE AMIP-II Reanalysis (R-2). *Bull. Amer. Meteorol. Soc.* **83**, 1631–1643 (2002).
64. Rippert, N. et al. Alternating influence of northern versus southern-sourced water masses on the equatorial Pacific subthermocline during the past 240 ka. *Paleoceanography* **32**, 1256–1274 (2017).
65. Parés, J. M. & Moore, T. C. New evidence for the Hawaiian hotspot plume motion since the Eocene. *Earth Planet. Sci. Lett.* **237**, 951–959 (2005).
66. Westerhold, T. et al. An astronomically dated record of Earth’s climate and its predictability over the last 66 million years. *Science* **369**, 1383–1387 (2020).
67. Rae, J. W. B. et al. Atmospheric CO₂ over the past 66 million years from marine archives. *Annu. Rev. Earth Planet. Sci.* **49**, 609–641 (2021).

Acknowledgements

We acknowledge the International Ocean Drilling Program for providing samples. We thank editors Joe Aslin and Sze Ling Ho and Ramon Egli and three anonymous reviewers for insightful suggestions that helped to improve the manuscript. We also thank CM² members and Dr. Hong Ao for useful discussions. This study was supported by the National Natural Science Foundation of China (92158208, 42261144739, 42274094, 4227040373), the opening foundation (SSKP202101) of the Shanghai Sheshan National Geophysical Observatory, Shanghai, China, the Shenzhen Science and Technology

Program (KQTD20170810111725321), the Australian Research Council (DP200100765), and the Special Funds for “Climbing program” (pdjh2022c0030 and pdjh2021c0024).

Author contributions

Q.S.L. supervised the project. D.F.W. designed the study and conceived the paper in discussion with A.P.R., E.J.R., and Q.S.L. W.Q.Y., Y.Z., Z.Q.Y., and Y.L. contributed to the laboratory assistance and manuscript refinement. All authors read and approved the final manuscript.

Competing interests

The authors declare no competing interests.

Additional information

Supplementary information The online version contains supplementary material available at <https://doi.org/10.1038/s43247-023-00702-y>.

Correspondence and requests for materials should be addressed to Qingsong Liu.

Peer review information *Communications Materials* thanks Toshitsugu Yamazaki, Ramon Egli and the other, anonymous, reviewer(s) for their contribution to the peer review of this work. Primary Handling Editors: Sze Ling Ho and Joe Aslin.

Reprints and permission information is available at <http://www.nature.com/reprints>

Publisher’s note Springer Nature remains neutral with regard to jurisdictional claims in published maps and institutional affiliations.



Open Access This article is licensed under a Creative Commons Attribution 4.0 International License, which permits use, sharing, adaptation, distribution and reproduction in any medium or format, as long as you give appropriate credit to the original author(s) and the source, provide a link to the Creative Commons license, and indicate if changes were made. The images or other third party material in this article are included in the article’s Creative Commons license, unless indicated otherwise in a credit line to the material. If material is not included in the article’s Creative Commons license and your intended use is not permitted by statutory regulation or exceeds the permitted use, you will need to obtain permission directly from the copyright holder. To view a copy of this license, visit <http://creativecommons.org/licenses/by/4.0/>.

© The Author(s) 2023